WATER RESOURCES RESEARCH, VOL. 49, 3712–3728, doi:10.1002/wrcr.20314, 2013

Impact of aquifer heterogeneity structure and local-scale dispersion on solute concentration uncertainty

Veljko Srzic,[1,2] Vladimir Cvetkovic,[1] Roko Andricevic,[2] and Hrvoje Gotovac[2]

Received 9 July 2012; revised 21 March 2013; accepted 12 May 2013; published 21 June 2013.

[1] In this paper, we study the influence of high log-conductivity variance (σ_Y^2) and local-scale dispersion on the first two concentration moments as well as on higher-order moments, skewness, and kurtosis, in a 2-D heterogeneous aquifer. Three different heterogeneity structures are considered, defined with one and the same global isotropic Gaussian variogram. The three structures differ in terms of spatial connectivity patterns at extreme log-conductivity values. Our numerical approach to simulate contaminant transport through heterogeneous porous media is based on the Lagrangian framework with a reverse tracking formulation. Advection and local-scale dispersion are two competing and controlling mechanisms, with a relative ratio defined by the Peclet number (Pe); hydraulic log-conductivity variance σ_Y^2 in the simulations is assumed to be one or eight. The term local-scale dispersion is used as a combined effect of molecular diffusion and mechanical dispersion. Uncertainty of the concentration field is quantified by the second-order moment, or the coefficient of variation (CV_C) as a function of the sampling position along a centerline, Peclet number, and σ_Y^2, as well as by higher-order moments, i.e., skewness and kurtosis. The parameter σ_Y^2 shows a strong influence on the concentration statistics, while the three different structures have a minor impact in the case of low heterogeneity. The results also indicate that for $\sigma_Y^2 = 8$, the influence of local-scale dispersion is significant after five integral scales (I_Y) from the source for the connected (CN) field, while in case of a disconnected field, the local-scale dispersion effect is observed after $20I_Y$ from the source. In the case of unit σ_Y^2, local-scale dispersion acts very slowly affecting concentration uncertainty at distances higher than $20I_Y$ from the source. Our inspection of Monte Carlo concentration skewness and kurtosis with the ones obtained from the Beta distribution show the discrepancies for high σ_Y^2 and CN log-conductivity structure.

Citation: Srzic, V., V. Cvetkovic, R. Andricevic, and H. Gotovac (2013), Impact of aquifer heterogeneity structure and local-scale dispersion on solute concentration uncertainty, *Water Resour. Res.*, *49*, 3712–3728, doi:10.1002/wrcr.20314.

1. Introduction

[2] Concentration fluctuations and their estimation in groundwater plumes have received increased attention in the last 20 years, since knowing the statistical properties of concentration fluctuations in a moving plume is important for risk assessment. Risk assessment studies require knowing the concentration fluctuations [*Andricevic et al*., 2012; *Tartakovsky*, 2007], which are completely described by a one-point concentration probability density function (PDF). At any point in space and time the concentration PDF contains all the information about concentration fluctuation phenomenology and embodies all the higher-order concentration moments of the stochastic process.

[3] The analyses of concentration moments and PDF in heterogeneous aquifers have been considered in a large number of studies. In the early attempts of characterizing groundwater contaminant transport, *Dagan* [1982] showed that in the absence of local-scale dispersion and a uniform source concentration, for the point sampling the concentration PDF is a two-state process of initial concentration, C_0, or zero. *Bellin et al*. [1994] analyzed the concentration cumulative distribution function (CDF) and first two concentration moments together with the coefficient of variation (CV_C) as a function of sampling volume. They demonstrated the influence of sampling volume on concentration moments, CV_C, and consequently the PDF shape. Neither of the studies incorporated local-scale dispersion as a mechanism for modifying the two-state concentration PDF, which may strongly influence the concentration variance, σ_Y^2, as well as higher concentration moments [*Andricevic*, 1998; *Dagan and Fiori*, 1997; *Fiori and Dagan*, 2000; *Kapoor and Kitanidis*, 1998].

[4] *Fiorotto and Caroni* [2002] considered the effect of local-scale dispersion in the case of wide ranges of sampling

[1]Department of Land and Water Resources, Royal Institute of Technology, Stockholm, Sweden.
[2]Department of Water Resources, Faculty of Civil Engineering, Architecture and Geodesy, University of Split, Split, Croatia.

Corresponding author: V. Srzic, Department of Water Resources, Faculty of Civil Engineering, Architecture and Geodesy, University of Split, Matice hrvatske 15, 21000 Split, Croatia. (veljko.srzic@gradst.hr)

0043-1397/13/10.1002/wrcr.20314

size, as well as for longitudinal source dimension, and demonstrated that numerical results compare well with an analytical solution for the first two concentration moments in low heterogeneity cases. *Caroni and Fiorotto* [2005] extended the analysis of *Pe* value influence on the concentration moments to cases characterized by $\sigma_Y^2 \leq 2$. They show that local-scale dispersion affects the concentration variance strongly, while the mean stays unaffected except for very low *Pe* values $O(10^1)$, which is in agreement with results in the literature [*Andricevic*, 1998; *Dagan and Fiori*, 1997; *Fiori and Dagan*, 2000; *Tonina and Bellin*, 2008]. *Dagan and Fiori* [1997] and *Fiori and Dagan* [2000] quantified the influence of local-scale dispersion on the first two concentration moments. Their finding is consistent with the analysis of field data by *Fitts* [1996], and they concluded that the concentration mean is weakly affected by local-scale dispersion. CV_C is also analyzed by *Fiori* [2003] and *Tonina and Bellin* [2008] as a function of the *Pe* number and the source size. Both the local-scale dispersion and source size result in decreasing the concentration variance and CV_C. *Bellin et al*. [1994] demonstrated how the increase in sampling volume decreases the concentration uncertainty, particularly at plume boundaries, but this analysis did not account for the effect of local-scale dispersion.

[5] The impact of sampling volume, local-scale dispersion, heterogeneity variance, and source size on the first two concentration moments, and CV_C, using first-order theory [*Dagan and Fiori*, 1997; *Fiori and Dagan*, 2000] and numerical results combined with analytical solutions derived as a generalization of the first-order solution for a finite sampling volume, are demonstrated in *Tonina and Bellin* [2008]. It was shown that the first-order theory based on analytical solutions are in good agreement with numerical results for σ_Y^2 values up to one and can be used to estimate the concentration uncertainty.

[6] *Caroni and Fiorotto* [2005] showed a good fit of the Beta distribution with Monte Carlo (MC) results conducted in a 2-D heterogeneous aquifer. *Bellin and Tonina* [2007] confirmed results by *Caroni and Fiorotto* [2005] and showed that the Ito stochastic differential equation (SDE) leads to a Beta distribution. By setting the *Pe* value equal to infinity, SDE converges to the double Dirac's concentration PDF showed by *Dagan* [1982]. *Schwede et al*. [2008] applied a semianalytical method and confirmed a very good agreement with Beta, even in 3-D, for different sampling volumes. A joint velocity-concentration PDF method has been developed by *Meyer et al*. [2010]. This method is much more efficient in comparison with standard MC, but the accuracy starts to deteriorate for $Pe \leq 100$. An additional attempt to derive methods based on the relationship between velocity distribution and concentration PDF has been presented by *Dentz and Tartakovsky* [2010]. These studies indicate the asymmetric shape of concentration PDF [*Cirpka et al*., 2011b], for a wide range of *Pe* values and sampling sizes, independent of distance from the source.

[7] The study of concentration statistics in heterogeneous aquifers in the past few decades has mostly been limited to the lower range of aquifer heterogeneity $\left(\sigma_Y^2 < 2\right)$ and to the common multi-Gaussian (MG) log-conductivity structure. The exception is work by *Meyer and Tchelepi* [2010] where σ_Y^2 up to four is considered as well as a non-Gaussian field characterized by significant correlation of high-value log-conductivity zones. The investigation of *Zinn and Harvey* [2003] opened possibilities for addressing different non-Gaussian heterogeneity structures departing from the MG one in a simple manner, whereas recent numerical advancements enable more reliable computations of advective transport in aquifers with high heterogeneity [*Gotovac et al*., 2007, 2009a].

[8] In this paper, we investigate the impact of different hydraulic log-conductivity structures and large variability on the solute plume uncertainty as quantified by the concentration mean, CV_C, skewness, and kurtosis. The MG field is considered as a base case, with two possible non-Gaussian fields [*Zinn and Harvey*, 2003] characterized by different correlations of extreme log-conductivity patterns. Furthermore, we contrast the case of low/moderate and high heterogeneity of the hydraulic conductivity by considering σ_Y^2 equal to one or eight, utilizing the numerical methodology of *Gotovac et al*. [2007, 2009a]. A particular issue to be addressed here is the spatial-temporal scale when local-scale dispersion becomes an important factor in estimating concentration uncertainty, and the validity of the Beta distribution as an approximation for evaluating concentration skewness and kurtosis.

2. Physical Statement of the Problem

[9] In this paper we consider incompressible and steady groundwater flow taking place through a heterogeneous aquifer and result in divergence free flow $\nabla \cdot \mathbf{v}(\mathbf{x}) = 0$. Velocity vector is defined on a finite sampling volume, in the vicinity of $\mathbf{x}$, which corresponds to Darcy scale. Because of aquifer heterogeneity, the seepage velocity $\mathbf{v}(\mathbf{x})$ is a random space function.

[10] If mass M of a conservative tracer is introduced into the aquifer, resident concentration needs to satisfy the mass conservation law

$$\frac{\partial c(\mathbf{x},t)}{\partial t} = -\nabla \cdot [\mathbf{v}(\mathbf{x})c(\mathbf{x},t)] + \nabla \cdot [\mathbf{D}(\mathbf{x})\nabla c(\mathbf{x},t)]. \qquad (1)$$

[11] The total change of conservative tracer mass in a finite aquifer volume is controlled by two mechanisms, advection and local-scale dispersion. The advection acts on relatively short time scales, to thin the contaminant plume and create lenses and fingers at its fringe. Local-scale dispersion acts irrespectively of the velocity random field, controlled by concentration gradients inside the plume domain. The parameter $c(\mathbf{x},t)$ denotes the concentration scalar field, defined as the contaminant mass per aquifer volume in the vicinity of $\mathbf{x}$ at time t. Local-scale dispersion is defined by $\mathbf{D}(\mathbf{x}) = D_m\mathbf{I} + \alpha\mathbf{v}(\mathbf{x})$, where $D_m\mathbf{I}$ quantifies molecular diffusion and α is a constant dispersivity.

[12] For initial time, concentration $c(\mathbf{x},0)$ is equal to C_0 inside the source area, while outside it takes zero value. For this study instantaneous resident injection mode is considered.

3. Numerical Methodology

3.1. Random Walk Particle Tracking

[13] For the purpose of this paper, the random walk particle tracking (RWPT) method is used to simulate

conservative tracer transport in a heterogeneous aquifer. RWPT is a method derived from stochastic physics, commonly used in the research of diffusion and dispersive processes in porous media [*Kinzelbach and Uffink*, 1986].

[14] If a total mass introduced in a heterogeneous aquifer is divided into a large number of particles of equal mass, then the movement of each particle is described in traditional form given by the Ito-Taylor integration scheme [*Ito*, 1990]

$$\mathbf{X}_P(t+\Delta t) - \mathbf{X}_P(t) = [\mathbf{v}(\mathbf{X}_P,t) + \nabla \cdot \mathbf{D}(\mathbf{X}_P,t)] \cdot \Delta t + \mathbf{B}(\mathbf{X}_P,t) \cdot \xi(t)\sqrt{\Delta t}, \quad (2)$$

where the first term on the right-hand side is the drift vector, while the displacement matrix $\mathbf{B}(\mathbf{X}_P;t)$ defines the strength of local-scale dispersion, and $\xi(t)$ presents a vector of independent, normally distributed random variables with zero mean and unit variance.

[15] As can be seen from equation (2), it is straightforward to calculate particle displacement because of the explicit time integration scheme. If the starting position of a contaminant particle is known, equation (2) calculates particle displacement resulting from advection and local-scale dispersion. Resident concentration [*Parker and van Genuchten*, 1984] is calculated from known particle displacement using smoothing techniques [*Hassan et al.*, 2001].

3.2. Adaptive *Fup* Monte Carlo Method (AFMCM)

[16] Despite all the advantages of the RWPT methodology [*Kinzelbach and Uffink*, 1986; *Salamon et al.*, 2006], it is difficult to calculate the $\mathbf{D}(\mathbf{X}_P;t)$ value. Solving the flow within an Eulerian framework using the usual numerical methods such as finite element method or Finite difference yields discontinuities in head as well as the velocity field. In equation (2), the $\mathbf{D}(\mathbf{X}_P;t)$ derivative cannot be accurately calculated if the above-mentioned methods are used without additional improvements [*LaBolle et al.*, 1996; *Salamon et al.*, 2006] designed to satisfy the mass conservation law. To avoid difficulties in mass conservation, we solve the flow and transport here in two dimensions using the proven AFMCM numerical methodology [*Gotovac et al.*, 2007, 2009a], which has been shown to converge and to be accurate even for high log-conductivity values.

[17] At its core, AFMCM is a collocation method that is combined with *Fup* basis functions defined on compact support, allowing us to compute the dispersion term and all its derivatives independently of the position vector. *Fup* collocation transform (FCT), closely related to the discrete Fourier transform, is required for the multiresolution representation of all flow and transport variables. The theoretical and practical aspects of AFMCM and FCT are presented in detail elsewhere [*Gotovac et al.*, 2007, 2009a]. All relevant variables such as log-conductivity, velocity, head or velocity, and concentration have a particular adaptive grid describing these on all spatial and temporal scales with a predefined accuracy level. An adaptive technique is used by adding a number of *Fup* basis functions in domain areas according to numerical adaptive criteria. To summarize, the most significant property of this method is the continuity of all variables and their derivatives.

3.3. Numerical Application

[18] In the case of backward random walk particle tracking (BRWPT), equation (2) can be used for calculating particle displacement as the starting position of each particle. Particles are distributed over a sampling volume, with a dimension smaller than the integral scale of log-conductivity and using a reverse scheme, are tracked back from detection volume to the contaminant source. In comparison with the forward scheme, the backward scheme possesses considerable simplifications in numerical calculation and evaluation whenever the sampling volume is much smaller than the source volume [*Fiorotto and Caroni*, 2002; *Caroni and Fiorotto*, 2005]. The number of particles N_P is distributed normally or uniformly in the detection volume and tracked back toward the source direction using equation (2). If n of total number of particles N_P released from the detection volume, in any time step Δt, is found inside the source volume, the concentration is evaluated as

$$C = C_0 \frac{n}{N_P}, \quad (3)$$

where C_0 presents the initial concentration when all released particles are found inside the source volume. In the BRWPT scheme, the source dimension is set up to be larger than the sampling volume. In the longitudinal direction, the source size dimension is $L_1 = 2I_Y$, while in the transverse direction it is $L_2 = 10I_Y$. Three different types of conductivity fields may result in highly different flow and mass transfer properties [*Zinn and Harvey*, 2003; *Wen and Gomez-Hernandez*, 1998] and are selected to analyze their influence on contaminant concentration statistical properties. All three structures have identical lognormal univariate conductivity distributions, as well as isotropic spatial covariance functions. They differ in the pattern by which high- or low-conductivity regions are connected:

[19] (1) ConNected: CN field with well-connected high-conductivity channels but poorly connected low- and mean-conductivity zones. This type of structure is characterized by an effective conductivity greater than the geometric mean and large variations in fluid velocity.

[20] (2) DisconNected: DN field, with well-connected low-conductivity zones such that transport occurs through low values of conductivity. This type of structure is characterized by an effective conductivity less than the geometric mean and smaller velocity variations.

[21] (3) Multi-Gaussian: MG field, where extreme conductivity values are poorly connected, while mean-conductivity zones are well connected. Only for this structure, the effective conductivity is equal to the geometric mean (for 2-D flow case) that is consistent with first-order theory.

[22] The CN and DN fields were generated through a transformation of the MG field in four basic steps: (i) the absolute value of the MG field (zero mean, unit variance) was calculated. This transform shifts extreme values to become high values, and values originally close to the mean become low values; (ii) the histogram of the values in the field was converted back to a univariate Gaussian distribution by mapping the CDF value at each point to a standard normal CDF; (iii) the block size of the field was increased such that the integral scale matched that of the

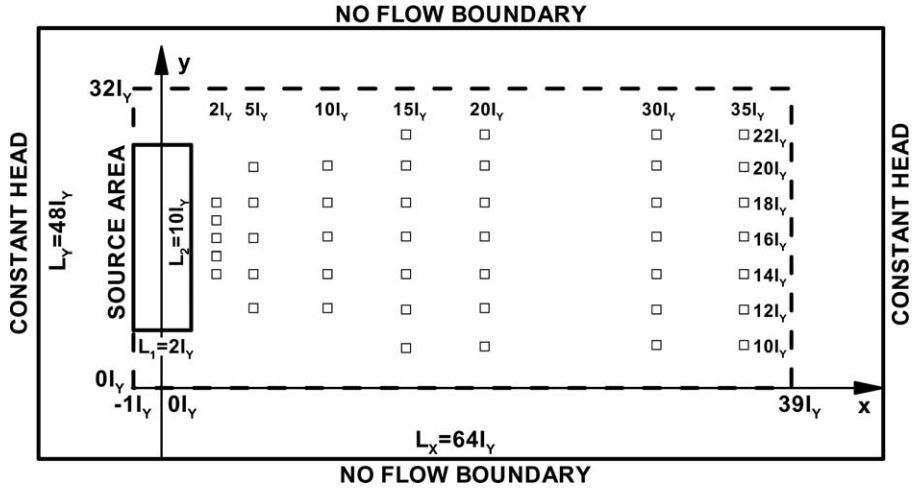

Figure 1. Numerical setup.

original MG field. This provided the final DN field; (iv) the CN field was then generated from the DN field by reflecting the values of the DN field around the mean.

[23] In this paper, we use the numerical setup properties shown in Figure 1 in order to explore the impact of different σ_Y^2, log-conductivity structure and *Pe* on concentration statistics. For the flow solution we use a domain $64I_Y \times 48I_Y$ ($I_Y = 16$ m). To avoid direct boundary effects, transport is simulated inside an inner domain, $8I_Y$ from upper and lower no-flux boundaries, and $12I_Y$ away from left- and right-side constant head boundaries. For the same numerical setup as in *Gotovac et al*. [2009b], inspection of the velocity variance in both longitudinal and transversal directions confirms that the boundary effects are small even for the highest variance, i.e., $\sigma_Y^2 = 8$. In comparison, *Salandin and Fiorotto* [1998] used $4I_Y$ to reduce the boundary effects, while *Janković et al*. [2003] separate flow and the inner domain with $10I_Y$. To achieve statistical confidence, MC convergence tests were conducted (Appendix A). Five hundred statistically independent realizations are considered as sufficient for concentration moments in the case of $\sigma_Y^2 = 1$, while for $\sigma_Y^2 = 8$ the required number of realizations is 2500. Transport is simulated by releasing 400 uniformly distributed particles from each of the 43 sampling volumes with instantaneous resident injection mode. Spatial discretization corresponds to a scale $I_Y/4$, the same as the sampling volume. We define this spatial discretization based on the grid convergence analysis summarized in Appendix B. The parameter σ_Y^2 is set up to be one or eight for three types of log-conductivity structures [*Zinn and Harvey*, 2003] with an isotropic Gaussian variogram. Effects of local-scale dispersion are analyzed for *Pe* number 100 or 10,000; the latter value is representative of advection-dominated transport. The dispersion tensor used here is simplified as an isotropic, velocity independent one.

[24] According to previous sections, we summarize the numerical procedure in five steps:

[25] (1) Generate a random hydraulic log-conductivity field with defined statistical properties using HYDRO-GEN [*Bellin and Rubin*, 1996]. The *Fup* regularized transform [*Gotovac et al*., 2007, 2009a] is used for data or function (e.g., log-conductivity) approximations in the same multiresolution fashion as FCT, but computationally more efficient.

[26] (2) Evaluate the Eulerian velocity and head field using the adaptive *Fup* collocation method inside the numerical domain with defined boundary conditions solving the flux balance equation.

[27] (3) Evaluate particle displacement at any time step using equation (2) with the BRWPT algorithm based on the Runge-Kutta-Verner explicit time integration scheme.

[28] (4) Evaluate resident concentration using equation (3).

[29] (5) Perform MC processing, which yields the statistical characterization of the concentration field in space and time.

3.4. Model Verification

[30] The numerical procedure explained in the previous section is used to simulate conservative contaminant transport in heterogeneous porous media. For the purpose of method verification, the numerical setup used here is presented in Figure 1, while the model parameters are chosen to be similar to those of *Caroni and Fiorotto* [2005]. The random log-conductivity field is a MG one, generated using HYDRO-GEN [*Bellin and Rubin*, 1996], and modeled with an isotropic exponential variogram.

[31] We focus the verification on spatial moments and analyze moment values along the centerline. In each rectangular sampling volume, 400 particles are uniformly distributed and tracked back via a reverse particle tracking scheme toward the source direction. The source dimension in the longitudinal direction is selected to be $L_1 = 2I_Y$, while in the transverse it is equal to $L_2 = 10I_Y$, approximately being ergodic. Simulations are made for $Pe = 100$ and 10,000, and $\sigma_Y^2 = 1$ with an constant anisotropic dispersion $D_Y = D_X/20$. The total number of MC realizations is 1000, and derived statistical moments (mean and standard deviation) are verified with previous numerical results [*Caroni and Fiorotto*, 2005].

[32] Figures 2a and 2c presents the verification of the concentration mean developed from numerical model results and one used in the analysis of *Caroni and Fiorotto*

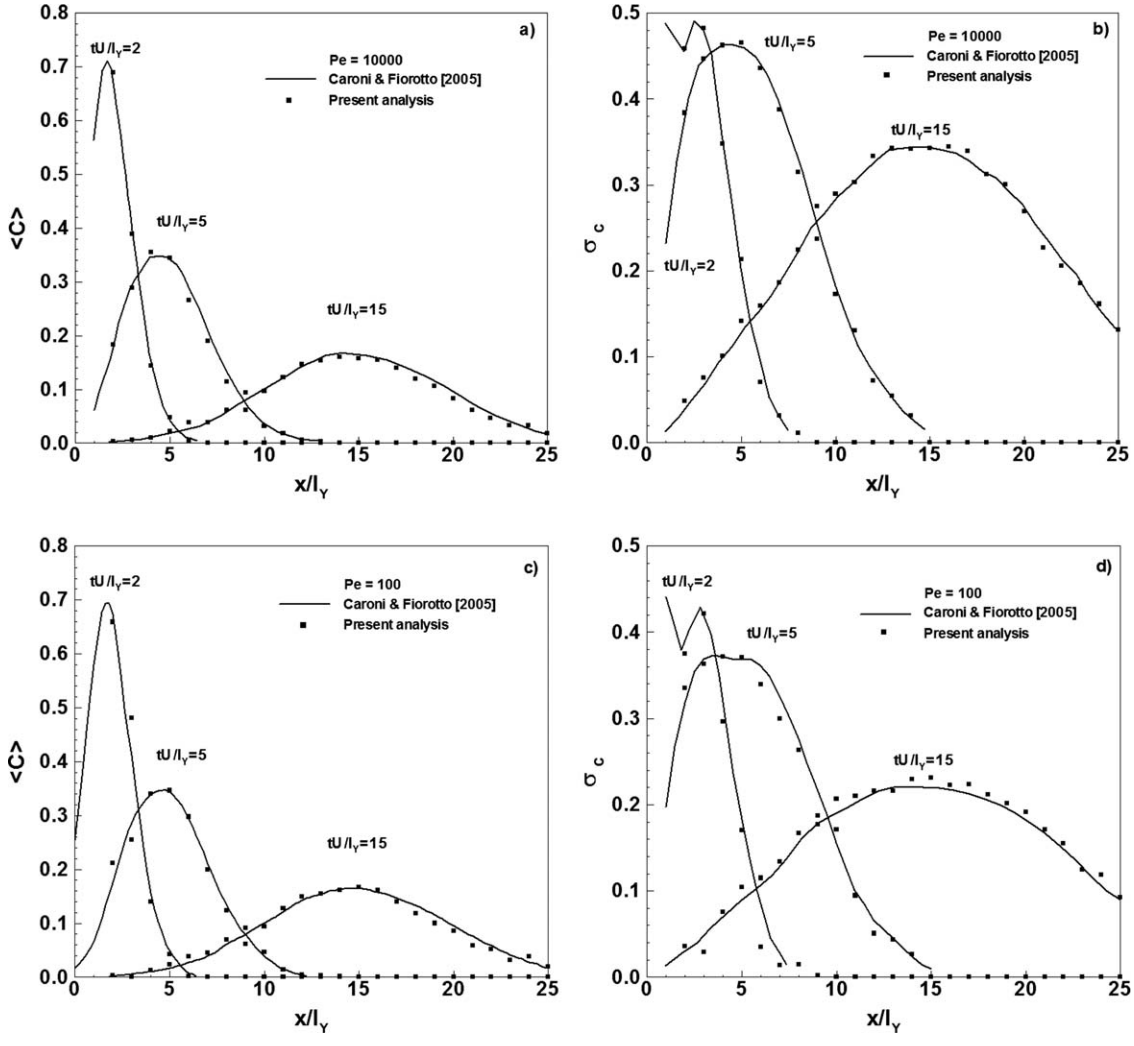

Figure 2. Model verification with *Caroni and Fiorotto* [2005]. $\sigma_Y^2 = 1$, MG field: (a) concentration mean along centerline for $tU/I_Y = 2$, 5, and 15, $Pe = 10{,}000$, (b) concentration standard deviation along centerline for $tU/I_Y = 2$, 5, and 15, $Pe = 10{,}000$, (c) concentration mean along centerline for $tU/I_Y = 2$, 5, and 15, $Pe = 100$, and (d) concentration standard deviation along centerline for $tU/I_Y = 2$, 5, and 15, $Pe = 100$.

[2005] for three different dimensionless times $tU/I_Y = 2$, 5, and 15 along the centerline, for $Pe = 10{,}000$ and 100. One can see good matching between the MC results conducted and ones by *Caroni and Fiorotto* [2005], independently of dimensionless times selected. For larger travel times since injection, the results obtained from the numerical procedure explained earlier are shown to be less smooth compared to early travel times. The cause of this may be found in an insufficient number of realizations. With an increasing number of realizations, smoothness would improve and reach levels similar to those of $tU/I_Y = 2$.

[33] Figures 2b and 2d present verification results of the concentration standard deviation. The bimodal feature is still well captured independently of the *Pe* value. It is important to notice the bimodal concentration standard deviation even for $tU/I_Y = 5$ in the case of smaller *Pe*, for both MC results and *Caroni and Fiorotto* [2005] results.

[34] To summarize, we show that our numerical procedure captures all key features related to contaminant transport, including bimodality in the concentration standard deviation, which vanishes for larger travel times. It is shown that our numerical procedure is able to balance between advection and local-scale dispersion as key transport mechanisms.

4. Results and Discussion

4.1. Effect of the Log-Conductivity Structure on Concentration Uncertainty

[35] Although three different log-conductivity fields, MG, DN, and CN, share the same overall spatial statistical properties, their differences in correlation structures affect the spatial and temporal concentration distributions, particularly in the case of high heterogeneity. We consider $Pe = 10{,}000$ as representative of an advection-dominated transport case in order to specifically analyze the influence of the log-conductivity field and σ_Y^2 on the first two concentration moments due to stretching, squeezing, and

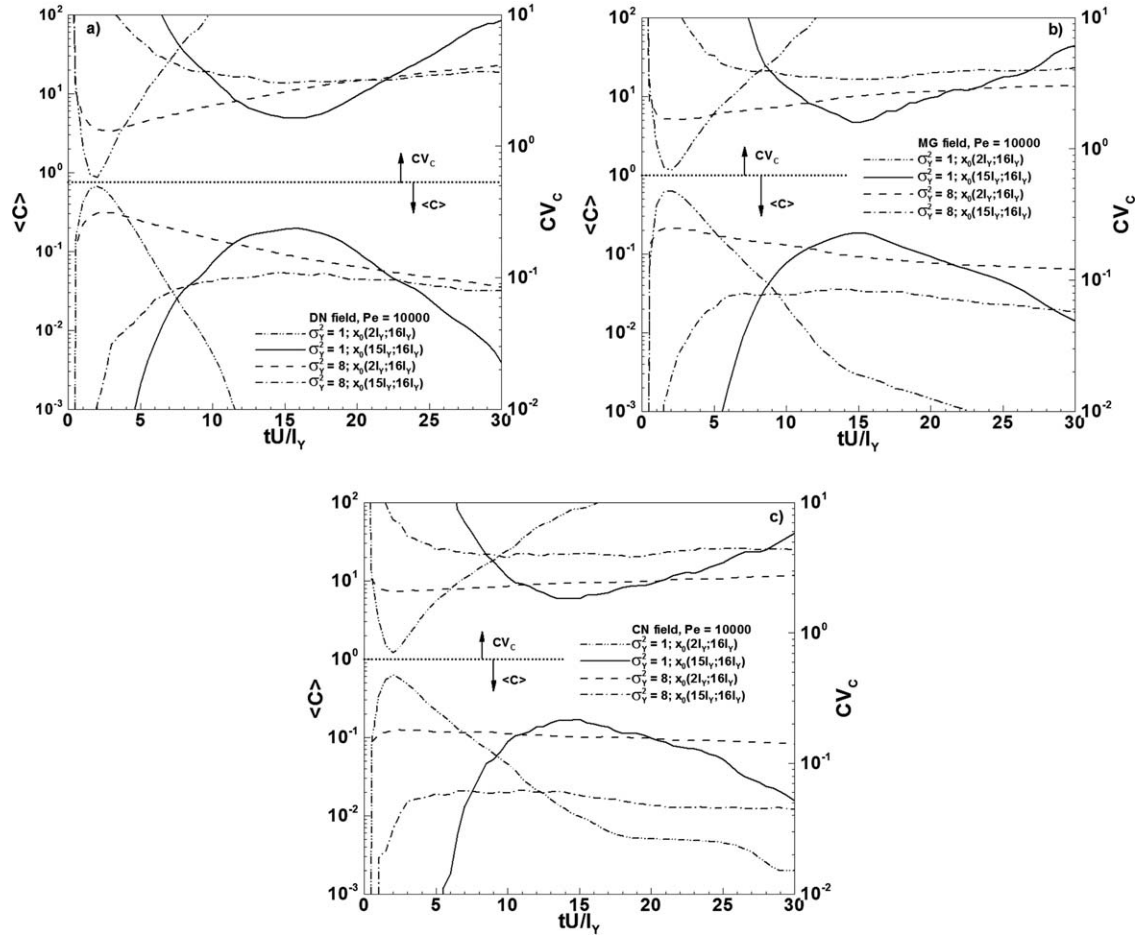

Figure 3. Concentration mean and CV_C for $Pe = 10{,}000$ at two different sampling locations 2 and 15 integral scales away from source center along centerline: (a) DN field, (b) MG field, and (c) CN field.

dispersing of the concentration plume mainly due to the advection. The analysis is performed at two sampling locations along a centerline, at 2 and $15I_Y$ from the source, characterizing near- and far-field transport characteristics (Figures 3a–3c).

[36] Concentration statistics under uniform average flow are significantly influenced by heterogeneity patterns and uncertainty related to its definition and measure. Consequently, velocity statistics related to different heterogeneity structures directly affect concentration moments and its PDF. It is well known that low heterogeneity implies a relatively uniform velocity distribution causing different non-Gaussian fields to possess velocity statistics that do not converge to those obtained by the MG classical field [*Wen and Gomez-Hernandez*, 1998]. Hence, all transport variables including concentration statistics only differ slightly for all three structures in the case of low heterogeneity [*Zinn and Harvey*, 2003; *Wen and Gomez-Hernandez*, 1998]. However, larger heterogeneity is generally characterized by a channeling effect, where the main portion of contaminant mass flow is located only through the few narrow channels [*Gotovac et al*., 2009b; *Janković et al*., 2003, 2006]. This channeling effect involves larger velocity variability resulting in increasing the velocity variance [*Zinn and Harvey*, 2003] and Lagrangian velocity correlation [*Gotovac et al*., 2009b]. This is particularly true for the CN field, where flow channels are extremely fast and narrow having large longitudinal correlation lengths that can occupy significantly larger domain areas than for MG and, especially, DN fields. On the other hand, the DN field also shows the channeling effect, but with relatively low velocity values indicating much slower flow channels and relatively low velocity variability even for higher heterogeneity. *Zinn and Harvey* [2003] showed by examining the breakthrough curve (BTC) at any control plane from the source that the solute mass is observed firstly for the CN field, then for MG, and lastly for the DN field, implying different early and late arrivals, as well as the peak position for all three structures.

[37] In Figure 3a–3c we present the concentration mean as a function of dimensionless time at two sampling locations along the centerline, separately for each log-conductivity. Note that dimensionless time used in this paper is normalized by mean velocity calculated for each particular heterogeneity structure. *Zinn and Harvey* [2003] showed that this formulation of dimensionless time is different than real time because mean velocities are different for each structure. For instance, mean velocities are similar for $\sigma_Y^2 = 1$, but for high heterogeneity and $\sigma_Y^2 = 8$, CN and DN fields have 2.5 times higher and lower mean velocity than MG field, respectively. In the case of $\sigma_Y^2 = 8$, and effective porosity of 0.2, the mean velocity for the MG field

is $U = 1.1037 \times 10^{-7}$m/s. In the case of the CN field, the mean velocity value is 250% higher, while for DN it is reduced by the same percentage. In this way, dimensionless time represents the time needed for particle to exceed the distance given the actual mean velocity defined by each particular log-conductivity structure. For low heterogeneity, the difference in mean velocity between different log-conductivity structures is less apparent for all sampling locations, as has been shown in the past [*Wen and Gomez-Hernandez*, 1998; *Zinn and Harvey*, 2003].

[38] Regardless of the heterogeneity structure, a higher σ_Y^2 produces a smaller concentration mean (smaller peak value) and longer tailings. In other words, due to larger heterogeneity and consequently velocity variability, the plume is more spread. Transport processes in the CN field result in enhanced plume spreading due to the higher velocity variations in longitudinal direction and preferential channeling effects. In this case, the plume is spread more irregularly creating a larger surface area between the plume and the surrounding fluid. This increases contaminant mass transfer driven primary by the concentration gradient. As a consequence, a higher reduction in the mean plume peak is observed. The mass transfer caused by local-scale dispersion moves mass from one streamline to the neighboring one in a transversal direction. Transversal dispersion is shown to be relevant for enhanced contaminant mixing, and is related to the σ_Y^2 as shown in *Cirpka et al*. [2011a]. Due to the velocity variations between neighboring streamlines, the plume attached to the pathway with slower velocity (e.g., immobile zone) is captured, while the rest of the plume is driven along paths with higher velocity. This increases the plume spreading and results in more pronounced tailing effects characterizing the CN field. The CN field results in the early first arrival and lower concentration peak values.

[39] The DN field is characterized by a relatively larger portion of slower transport through the low-permeable areas, resulting in the later plume arrival compared to the case of MG or CN structures. As expected, the MG field positions itself between these two extreme non-Gaussian fields. On the other hand (under same conditions), on contaminant plume margins, the concentration moments are higher for higher heterogeneity, which is a result of the fact that the plume is spread over a larger area in these time intervals taking nonzero concentration values.

[40] Besides the concentration mean, within the same Figures 3a–3c, we present the concentration standard deviation through CV_C. Although we do not present standard deviation explicitly, our investigation through CV_C leads to the conclusion that standard deviation is also affected by both log-conductivity structure and variance. A bimodal feature in concentration variance is a unique property noticed at early travel times for $\sigma_Y^2 = 1$ in all log-conductivity structures. Our results in Figure 4 present the difference in concentration variance for CN and DN fields in the case $\sigma_Y^2 = 1$. We select the case with a higher *Pe* value, which reduces the influence of local-scale dispersion and highlights the influence of the conductivity structure. A bimodal feature of the concentration variance is more apparent in the case of a DN field. Velocity variations are lower than in the case of the CN field, which results in more pronounced plume overlapping between different realizations.

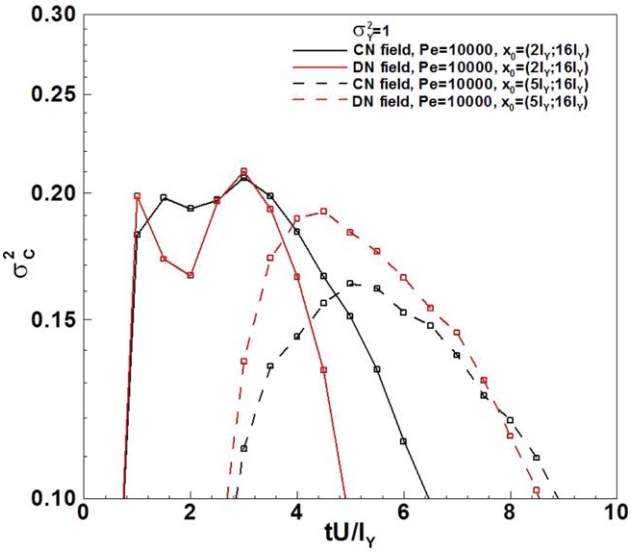

Figure 4. Bimodal feature in concentration variance for DN and CN field, $\sigma_Y^2 = 1$.

Also, for a purely advective case and point sampling, concentration variance is a function of the concentration mean and initial concentration $\sigma_C^2 = \langle C \rangle (C_0 - \langle C \rangle)$ [*Dagan*, 1982], providing an upper bound for concentration fluctuations. Related to this, if the concentration mean takes values greater than $C_0/2$, the bimodal feature is present (valid only for pure advection). Our results for concentration mean (Figures 3a–3c) show higher mean concentration values in the case of the DN field (even higher than $C_0/2$), which leads to a significant bimodal feature in the concentration variance; this is in contrast to the case of the CN field. For sampling $5I_Y$ away from the source, the bimodal feature vanishes for both cases (CN and DN). The peak concentration variance value is first observed for the CN field, based on higher mean velocity values.

[41] For later travel times, the plume is further dispersed and the concentration mean is lower. This results in reduced concentration variance values and a disappearance of the concentration variance bimodal feature. The bimodal feature is not present for the higher σ_Y^2 values for all three types of conductivity structures, including even the closest sampling location. This is in agreement with the results by *Caroni and Fiorotto* [2005] and *Tonina and Bellin* [2008].

[42] The concentration coefficient of variation is presented in Figures 3a–3c as a function of travel time. As expected, the lowest CV_C values are observed in the plume center, independently of the log-conductivity structure, because the plume shows similar properties over different realizations around the plume center. Contrary to this, the concentration estimation is more uncertain at the plume boundaries implying that advection meanders the plume (because of velocity variability characterizing scales greater than the source) around the center in an irregular way, especially for high heterogeneity. By comparing three different log-conductivity structures, CV_C shows the well-known "*U*" shape, which starts to be more skewed as the σ_Y^2 increases its value. The largest uncertainty level at the plume center is observed in the case of a CN field, which is reasonable considering the properties of concentration

mean and standard deviation as already explained, while the most reliable field for concentration prediction based on first two moments is the DN one. At the plume margins (corresponding to the first and late arrivals), a higher uncertainty level is observed in the DN field compared to the MG and CN fields.

[43] Regardless of log-conductivity structure, by comparing different σ_Y^2, the higher log-conductivity variance increases the uncertainty at the plume center and consequently decreases it at the plume fringes (contrary to unit σ_Y^2 case). Regarding the plume shape and size, uncertainty at the fringes is lower for higher σ_Y^2 (Figures 3a–3c). If one compares plume shape and size for two different log-conductivity variances ($\sigma_Y^2 = 1$ and 8), the conclusions arising from the comparison can be summarized as follows:

[44] (1) in the case of lower σ_Y^2, the plume shape is much more regular with less pronounced fringes and lenses, while the plume size is defined by aquifer heterogeneity resulting in different velocity values.

[45] (2) by increasing the σ_Y^2, velocity variations are more pronounced. This will cause the plume to be dispersed over a larger area with fringes found at preferential channels. In the case of unit σ_Y^2, the lowest concentration uncertainty is observed at the plume center, and it increases toward plume boundaries. This is explained as a consequence of frequent plume overlapping from realization to realization in the plume central part. Consequently, the overlapping will decrease as the sampler is closer to plume boundaries, which increases the uncertainty. The same explanation is valid even for higher σ_Y^2.

[46] Early arrivals are occurring faster in highly heterogeneous media due to the existence of extremely fast streamlines that significantly enhance plume spreading. On the other hand, the late arrivals are characterized through concentration moments with the strong tailing effect. This is more pronounced for the high heterogeneity and the CN structure due to slow (even "stacked") streamlines in low-permeable areas outside of the dominant flow channels. Generally, high heterogeneity CN fields exhibit larger differences in the first two concentration moments implying that connectivity patterns may have a dominant role for concentrations statistics, as also evidenced in many field sites (e.g., Macrodispersion Experiment (MADE)) [*Zheng et al*., 2010].

[47] Sensitivity of the concentration mean and variance to the sampling volume scale for DN and CN fields has been analyzed (Appendix C). In general, the concentration mean is little affected by changes in sampling volume irrespective of log-conductivity structure and σ_Y^2. By contrast, CV_C characterizing the CN field for high σ_Y^2 is significantly affected by the sampling volume scale, especially at the plume fringes.

4.2. Effects of Local-Scale Dispersion

[48] In this subsection, we analyze the effects of local-scale dispersion for all three structures considering low and high heterogeneity and particularly the time evolution of the local-scale dispersion impact on concentration uncertainty. Since real flow and transport processes are advection dominated, the concentration mean (especially peak) is not significantly affected by local-scale dispersion [*Andricevic*, 1998; *Dagan and Fiori*, 1997; *Fiori and Dagan*, 2000]. Therefore, we focus on the CV_C, which contrary to the mean, is affected by local-scale dispersion.

[49] In general, the local-scale dispersion always acts on the plume due to the concentration gradients, but its impact is closely related to the contact area between a plume and surrounding space measured by the *Pe* number. Advection is a dominant transport mechanism in porous media that stretches and meanders the plume rapidly, while local-scale dispersion is a relatively slow process acting simultaneously with advection but after a certain time may have an important influence on concentration statistics [*Andricevic*, 1998; *Andricevic*, 2008]. After some time, the impact of local-scale dispersion and advection balance each other, while their relationship is strongly influenced by the heterogeneity field (log-conductivity variance and correlation of different log-conductivity patterns). In the random walk context, the local-scale dispersion spreads particles from advective streamlines to the surrounding area. In low heterogeneity cases, due to relatively uniform velocity distribution, the local-scale dispersion slowly disperses a concentration plume requiring a lot of time before it significantly influences the concentration moments. By contrast, the local-scale dispersion in the high heterogeneous aquifers causes particles from the fast and narrow advective channels [*Cirpka et al*., 2011a] to transfer to the wider surrounding area with very small velocities resulting in a much faster influence on the concentration statistics. To the best of our knowledge, there is no reliable evidence about time evolution of local-scale dispersion impact in highly heterogeneous porous media for different non-Gaussian fields.

[50] In Figures 5a–5c, we demonstrate the influence of local-scale dispersion on CV_C in the case of three heterogeneity structures for both sampling positions (2 and $15I_Y$ at centerline far from the source) through the time. The local-scale dispersion acts as a reducing mechanism that disperses the plume intensively over the aquifer area and results in reducing uncertainty. Close to the source area, the influence of the local-scale dispersion on CV_C is not visible due to the fact that the dispersion process needs time to evolve and to reduce higher concentration gradients over the plume. Farther from the source (at $15I_Y$), the local-scale dispersion effect is more pronounced. According to the results presented in Figures 5a–5c, the plume center is still not affected by local-scale dispersion at this position in the case of lower σ_Y^2. The solid curve presenting the almost pure advective case ($Pe = 10{,}000$) fits well symbols presenting strong local-scale dispersion characterized by $Pe = 100$. For increased σ_Y^2, one can see higher values of concentration uncertainty in both the central and fringe parts of the plume. Advection strictly increases the concentration uncertainty independently of the sampling position while local-scale dispersion acts to decrease it.

[51] Further evidence of time evolution of the local-scale dispersion impact is presented in Figures 6a–6f for different dimensionless times (5, 10, 20, and 35) along the centerline. For unit σ_Y^2, the local-scale dispersion acts very slowly and after 20 dimensionless times (related to 20 integral scales in terms of mean velocity) starts to show some influence on the concentration uncertainty for the CN field,

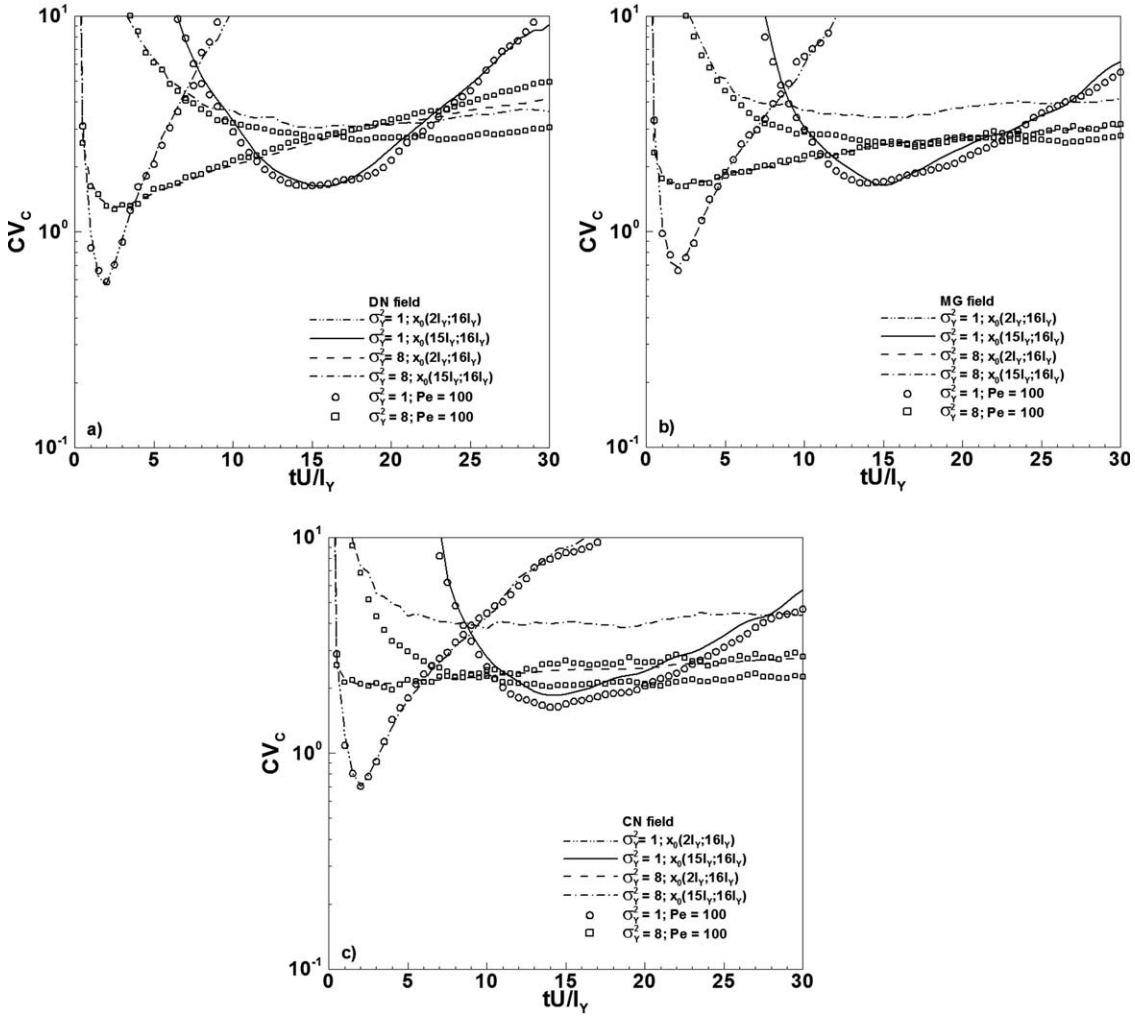

Figure 5. CV_C for $Pe = 10{,}000$ (lines) and $Pe = 100$ (symbols) at two different sampling locations 2 and 15 integral scales away from source center along centerline in case of (a) DN field, (b) MG field, and (c) CN field.

while in an MG field, the CV_C stays almost unaffected by local-scale dispersion even after 20 dimensionless times (Figures 6a, 6c, and 6e). Furthermore, the DN field stays unaffected by local-scale dispersion for a long time (35 dimensionless) after injection. Note that the concentration peak is especially weakly dependent on local-scale dispersion having a CV_C value between one and two for all three structures. We can conclude that differences between three heterogeneity structures are not so significant with respect to the influence of local-scale dispersion, and advection remains as a dominant transport mechanism for low heterogeneity [e.g., *Dagan and Fiori*, 1997; *Rubin*, 2003; *Tonina and Bellin*, 2008].

[52] On the other hand, Figures 6b, 6d, and 6f present a significant influence from the local-scale dispersion for highly heterogeneous porous media $\left(\sigma_Y^2 = 8\right)$. In this case, the local-scale dispersion reduces concentration uncertainty rapidly even close to the source. At a far distance and later times, local-scale dispersion with $Pe = 100$ considerably decreases the uncertainty level and reduces the CV_C to between one and two for all three fields. The local-scale dispersion has the most profound effect in the CN field, where connectivity patterns strongly influence the transport mechanisms [*Knudby and Carrera*, 2005]. In the case of a CN field, the preferential fast flow channels (created by connected high log-conductivity values) spread a plume rapidly over a larger space, drastically extending the contact area around and within the plume, thereby enhancing local-scale dispersion impact. In this case, the local-scale dispersion effect is already visible at the dimensionless time equal to five (Figure 6e). For the MG field, the local-scale dispersion effect becomes visible later, at 10 dimensionless time, while in the case of a DN field (Figure 6b) its influence becomes visible only after 20 dimensionless times from the injection.

4.3. Higher-Order Concentration Moments

[53] Recent studies of concentration PDF have shown that it is asymmetric in both spatial and temporal domains [*Bellin and Tonina*, 2007; *Cirpka et al*., 2011b; *Schwede et al*., 2008]. This implies that the first two moments (concentration mean and CV_C) do not provide sufficient information for characterizing the concentration PDF, stressing the need for higher-order concentration moments. Furthermore, the Beta distribution (characterized by the first two

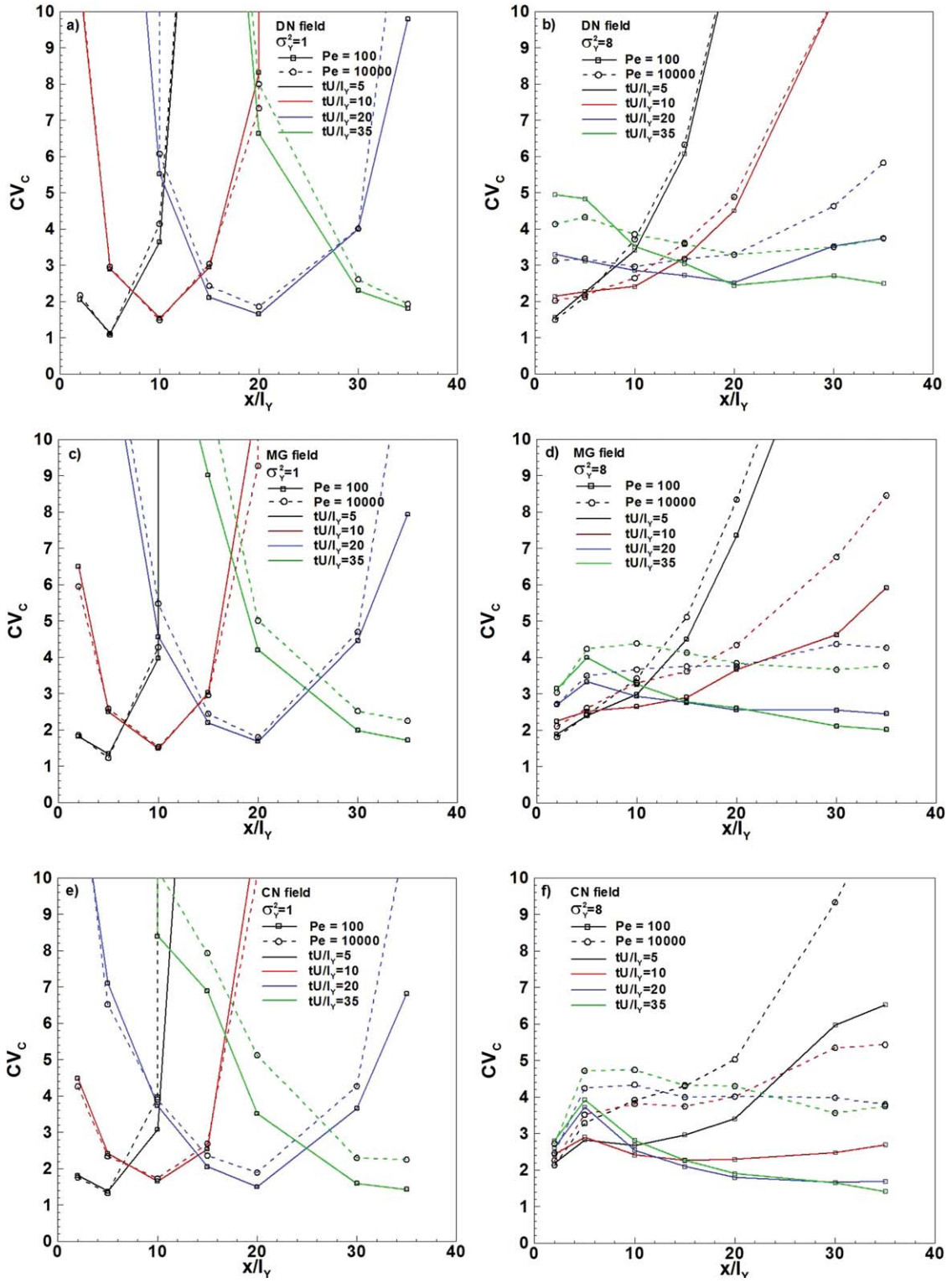

Figure 6. CV_C for $Pe = 10{,}000$ (dashed lines) and $Pe = 100$ (solid lines) at seven different sampling locations 2, 5, 10, 15, 20, 30, and 35 integral scales along centerline for selected times 5, 10, 20, and 35 dimensionless, in case of (a) DN field, $\sigma_Y^2 = 1$, (b) DN field, $\sigma_Y^2 = 8$, (c) MG field, $\sigma_Y^2 = 1$, (d) MG field, $\sigma_Y^2 = 8$, (e) CN field, $\sigma_Y^2 = 1$, and (f) CN field, $\sigma_Y^2 = 8$.

moments only) has been recommended as a suitable approximation for quantifying concentration fluctuations [*Bellin and Tonina*, 2007; *Caroni and Fiorotto*, 2005].

[54] In this section we illustrate the concentration skewness and kurtosis for CN and DN log-conductivity fields, with $\sigma_Y^2 = 1$ and 8 and make a comparison with skewness

Table 1. Concentration Skewness Comparison Between MC Results and Ones Obtained From Beta Distribution for CN and DN Log-Conductivity Structures, $Pe = 100$ and 10,000, Sampling Locations $2I_Y$ and $15I_Y$ From Source and Three Different Randomly Selected Snapshots

			Sampling Volume $2I_Y$ Away From Source						Sampling Volume $15I_Y$ Away From Source					
			$tU/I_Y = 1$		$tU/I_Y = 2$		$tU/I_Y = 8$		$tU/I_Y = 10$		$tU/I_Y = 15$		$tU/I_Y = 25$	
		Pe	100	10,000	100	10,000	100	10,000	100	10,000	100	10,000	100	10,000
Log-conductivity variance = 1	DN	MC	−0.11	0.20	−0.88	−0.90	7.75	7.47	2.98	3.23	1.61	1.45	6.05	5.92
		Beta distribution	−0.11	0.18	−0.88	−0.90	8.08	7.32	2.99	3.26	1.61	1.47	6.16	5.96
	CN	MC	0.40	0.63	−0.55	−0.51	3.23	3.06	2.90	2.75	1.97	1.72	4.25	4.00
		Beta distribution	0.41	0.65	−0.53	−0.51	3.25	3.03	2.93	2.86	1.89	1.73	4.09	3.92
Log-conductivity variance = 8	DN	MC	1.21	1.33	0.77	0.82	1.64	1.66	4.20	4.59	3.89	3.85	4.22	5.10
		Beta distribution	1.22	1.34	0.79	0.83	1.64	1.66	4.09	4.41	3.80	3.78	3.97	4.53
	CN	MC	2.23	2.35	2.26	2.22	2.40	2.33	4.17	5.94	3.57	7.54	5.14	9.19
		Beta distribution	2.29	2.39	2.27	2.22	2.37	2.33	3.92	5.73	3.70	6.10	3.99	6.98

and kurtosis as inferred from the Beta distribution that is obtained using the concentration mean and variance as calculated from MC statistics. The results for concentration skewness are presented in Table 1, while kurtosis values are shown in Table 2.

[55] At the plume center, higher σ_Y^2 leads to highly skewed distributions, while the opposite is true at the plume fringes. Irrespective of the Pe value, the local-scale dispersion has not sufficiently evolved for the nearest sampling at the plume center, and normalized concentration values higher than 0.5 are most frequently observed (negative skewness values). Contrary to the DN field, concentration PDF characterizing the CN field is more skewed toward zero concentration values for a purely advective case due to the frequent number of zero concentration values since transport occurs in relatively narrow channels. For dominant local-scale dispersion influence ($Pe = 100$) and $\sigma_Y^2 = 8$ characterizing the CN field, we notice lower skewed PDF in comparison to the DN case (in plume core for sampling $15I_Y$ from source). To explain this we must return to the previous section. According to Figures 6b and 6f, local-scale dispersion characterizing the CN field is much more pronounced than in the DN case. For $\sigma_Y^2 = 8$ local-scale dispersion is so dominant that a generalization of the log-conductivity structure and its influence on CV_C and concentration skewness cannot be accepted.

[56] As the distance from source increases, negative skewness values disappear. Also, due to the meandering effect at the plume boundaries, skewness increases and is positive. Concentration distribution at the plume fringes in the case of the CN field is characterized as less skewed than for the DN field due to a more pronounced tailing effect. The Pe value does not influence skewness significantly except for late travel time and the farthest sampling in the case of the CN field for a high heterogeneity case. Concentration kurtosis is influenced by the log-conductivity structure and local-scale dispersion in a similar manner as skewness. In peak values and for different σ_Y^2, the highest differences in kurtosis due to the local-scale dispersion are noticed for the CN structure. For early travel times, local-scale dispersion does not influence concentration kurtosis values (for unit σ_Y^2), which are similar for both CN and DN structures, especially in the plume core. At the plume fringes we note that the discrepancies between kurtosis values characterizing different log-conductivity structures are increasing in the same way as shown for skewness and CV_C. This phenomenon is more pronounced as the σ_Y^2 increases.

[57] Comparison of MC skewness and kurtosis with the ones obtained from the Beta distribution leads to the conclusion that Beta can accurately define both the concentration skewness and kurtosis for the samplings close to the source, even for $\sigma_Y^2 = 8$ and the CN field, within the whole time interval analyzed in the study. For sampling $15I_Y$ away from the source, however, Beta provides a close representation only if $\sigma_Y^2 = 1$. With a higher σ_Y^2, our results

Table 2. Concentration Kurtosis Comparison Between MC Results and Ones Obtained From Beta Distribution for CN and DN Log-Conductivity Structures, $Pe = 100$ and 10,000, Sampling Locations $2I_Y$ and $15I_Y$ From Source and Three Different Randomly Selected Snapshots

			Sampling Volume $2I_Y$ Away From Source						Sampling Volume $15I_Y$ Away From Source					
			$tU/I_Y = 1$		$tU/I_Y = 2$		$tU/I_Y = 8$		$tU/I_Y = 10$		$tU/I_Y = 15$		$tU/I_Y = 25$	
		Pe	100	10,000	100	10,000	100	10,000	100	10,000	100	10,000	100	10,000
Log-conductivity variance = 1	DN	MC	1.20	1.22	1.97	2.03	65.87	61.98	10.52	12.44	4.32	3.58	45.77	41.07
		Beta distribution	1.17	1.19	1.95	1.99	71.42	58.42	10.49	12.42	4.22	3.62	45.62	40.82
	CN	MC	1.36	1.58	1.46	1.42	11.87	10.69	10.72	9.35	6.09	4.47	23.51	18.83
		Beta distribution	1.33	1.58	1.41	1.40	11.93	10.49	10.85	9.90	5.57	4.46	20.79	17.71
Log-conductivity variance = 8	DN	MC	2.66	2.98	1.81	1.89	4.05	4.18	21.91	25.02	20.14	18.30	23.59	31.08
		Beta distribution	2.67	2.97	1.80	1.88	4.03	4.12	20.43	22.82	18.73	17.48	20.78	24.88
	CN	MC	6.92	7.59	7.05	6.88	7.57	7.29	29.29	45.28	20.86	75.48	51.67	118.06
		Beta distribution	7.04	7.64	6.99	6.74	7.33	7.16	23.07	42.35	21.53	47.21	25.02	63.01

suggest that the Beta distribution provides an accurate representation of the concentration PDF only for early times.

4.4. Concentration Statistics

[58] Concentration statistics rely on the first two concentration moments for low heterogeneity since *Caroni and Fiorotto* [2005] and *Tonina and Bellin* [2008] showed that a Beta distribution, under certain circumstances, can provide a good approximation of the concentration PDF for the MG field and log-conductivity variance up to two. For a high heterogeneity case, however, the concentration PDF depends on higher-order moments. Here we show and extend the potential usage of the Beta distribution as representative of the concentration PDF, for CN and DN log-conductivity structures; however, it seems necessary to include higher-order concentration moments in order to properly capture concentration fluctuations. *Yee* [2009] confirmed that under different conditions in transport media characterized by turbulence (in air tunnels and water channels), higher-order concentration moments can be defined as a function of the first two concentration moments only, by taking advantage of the moment collapse feature. One important question is whether it is possible to obtain moment collapse for different heterogeneity structures and *Pe* numbers in porous media. Moment collapse enables one to evaluate only the first two concentration moments in order to obtain all the needed higher-order moments and finally the complete concentration PDF. *Yee* [2008] also found that in turbulent diffusion, the usage of three or two-parameter PDFs such as a clipped gamma or exponential is useful for defining the full concentration PDF. We can conclude that our presented results quantify the influence of advection and local-scale dispersion under different conditions of heterogeneity in aquifers and can serve as a solid base for exploring moment collapse and the concentration PDF, which is a topic of ongoing research. Also, the analysis of concentration mean and CV_C, complemented by computations of the skewness and kurtosis, provide a solid foundation for further characterizing concentration fluctuations and the associated uncertainty.

[59] On the other hand, the concentration PDF accompanied by aquifer information is a key element for risk assessment [*Andricevic et al*., 2012]. Although a PDF contains all the information about spatial and temporal concentration values, regulatory policies use only maximum average concentration or reference dose values together with prescribed exposure duration as an input in human health risk assessment. Because of the concentration stochastic nature in heterogeneous aquifers, it is important to complete the information about concentration fluctuations. When this is aligned to aquifer characterization data, it will enable one to describe the necessary input for improving reliable estimations of risk probability. The statistical moment analysis presented in this paper allows a better understanding of different *Pe* values, log-conductivity variance values, and different spatially correlated structures and their influence on the concentration characterization used in risk assessment.

5. Conclusions

[60] In this paper, we analyze the influence of three spatial log-conductivity structures (MG and two non-Gaussian) with local-scale dispersion on the first two concentration moments and extend the analysis to skewness and kurtosis. We particularly focus on the influence of aquifer heterogeneity and temporal evolution of the local-scale dispersion impact considering a coefficient of variation as well as skewness and kurtosis as a measure of uncertainty. Although the research on concentration uncertainty has been extensive over the past decades, new results from this study can be helpful in determining uncertainty in in situ cases, recognizable by their distinctive properties that deviate from theoretical MG conductivity fields and in addition exhibit relatively high variability in hydraulic properties.

[61] Based on this work our general conclusion is that effect of local-scale dispersion on plume dilution and mixing over time depends on the log-conductivity structure and the degree of aquifer heterogeneity. A few specific concluding points we summarized as follows:

[62] (1) The main consequences of high heterogeneity are significant reduction in the concentration peak, shortened first arrival due to the higher velocity contrast, characterizing preferential channels, and enhanced tailing effect in BTCs.

[63] (2) Increasing heterogeneity yields higher uncertainty around the plume center and lower uncertainty at the plume edges, contrary to the case characterized by lower aquifer heterogeneity, due to different properties of plume's shape and size for low and high heterogeneity.

[64] (3) Although the existence of preferential channels causes more erratic plume shape, if accompanied by aquifer heterogeneity it contributes to enhanced plume mixing resulting in reduced concentration uncertainty (only for lower *Pe* values).

[65] (4) Inspection of concentration skewness and kurtosis indicated and confirmed the asymmetric and skewed shape of the concentration PDF. The total number of concentration moments required for accurate quantification of the plume fluctuations should be investigated further.

[66] (5) Beta distribution skewness and kurtosis have been shown to be in good agreement with MC results in the case of low heterogeneity; with increasing σ_Y^2, the divergence of skewness and kurtosis between simulations and the Beta model is more pronounced.

[67] Based on the results presented in this paper, a future challenge and possible extension of the paper would be to check the validity of the partially successful application of the Beta distribution [*Bellin and Tonina*, 2007; *Schwede et al*., 2008] for the low/mild and high heterogeneity cases. The current results for high heterogeneity cases indicate the potential importance of knowing the higher concentration moments in order to establish a potential relationship with lower-order ones. This relationship will lead one to a complete definition of the concentration PDF (based on information solely about lower-order moments), which is essential information for the risk assessment of groundwater contamination.

Appendix A: MC Convergence

[68] For analyzing higher-order normalized concentration moment convergence, we use the numerical setup as presented in Figure 1. MC convergence tests for

concentration mean and CV_C were conducted, as well as for higher-order moments (skewness and kurtosis), for $\sigma_Y^2 = 1$ and 8. The CN field with a higher velocity variance is chosen for illustration. Starting from 10, the number of realizations is increased until convergence in moment values is achieved. For this purpose we select two random samplings and dimensionless snapshots. The results of the MC convergence are presented later.

[69] First, we present MC convergence for $\sigma_Y^2 = 8$. The number of realizations increases until an asymptotic relative ratio (ratio between nth moment value calculated from N_R realizations and nth moment value calculated for highest number of realizations (2500)) is achieved. In Figures A1a–A1g, we present the results of MC convergence for $Pe = 100$ and 10,000, CN field and $\sigma_Y^2 = 8$. Sampling positions and snapshots are selected to capture the plume core as well as plume fringes due to the different convergence requirements. It can be seen that for all four concentration moments (mean, CV_C, skewness, and kurtosis), 2500 transport realizations are sufficient. The concentration mean (Figures A1a and A1b) shows increasing discrepancies toward plume boundaries, but even so, the differences between 2200 and 2500 MC are small irrespective of the Pe value.

[70] CV_C (Figures A1c and A1d) is shown to be stable even for 1500 MC realizations (differs less than 1% contrary to 2500 MC). A greater difference between plume core and peripheral part has not been observed. In contrast

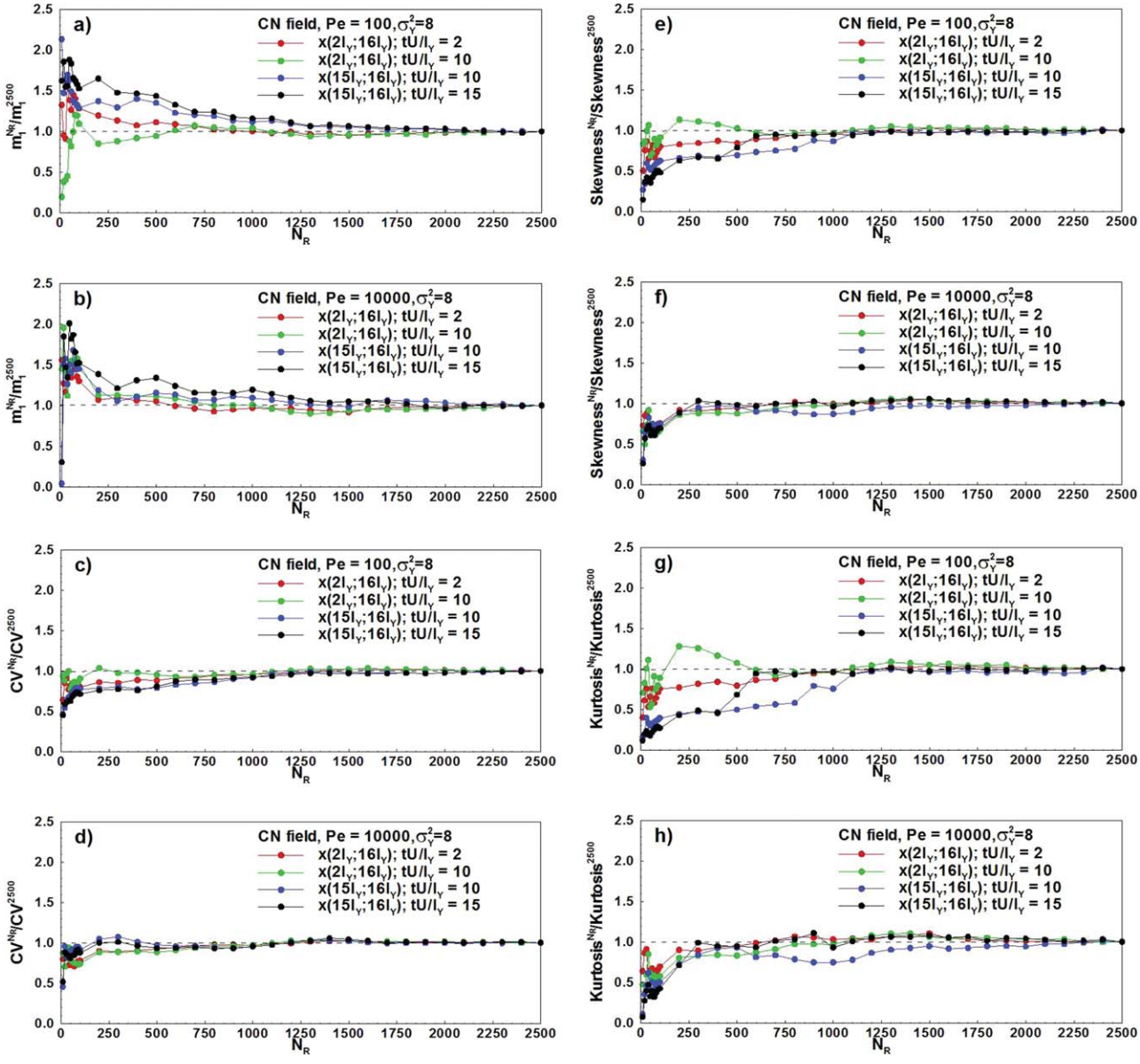

Figure A1. MC convergence study results in case of $\sigma_Y^2 = 8$, CN field; (a) concentration mean, $Pe = 100$, (b) concentration mean, $Pe = 10{,}000$, (c) CV_C, $Pe = 100$, (d) CV_C, $Pe = 10{,}000$, (e) concentration skewness, $Pe = 100$, (f) concentration skewness, $Pe = 10{,}000$, (g) concentration kurtosis, $Pe = 100$, and (h) concentration kurtosis, $Pe = 10{,}000$.

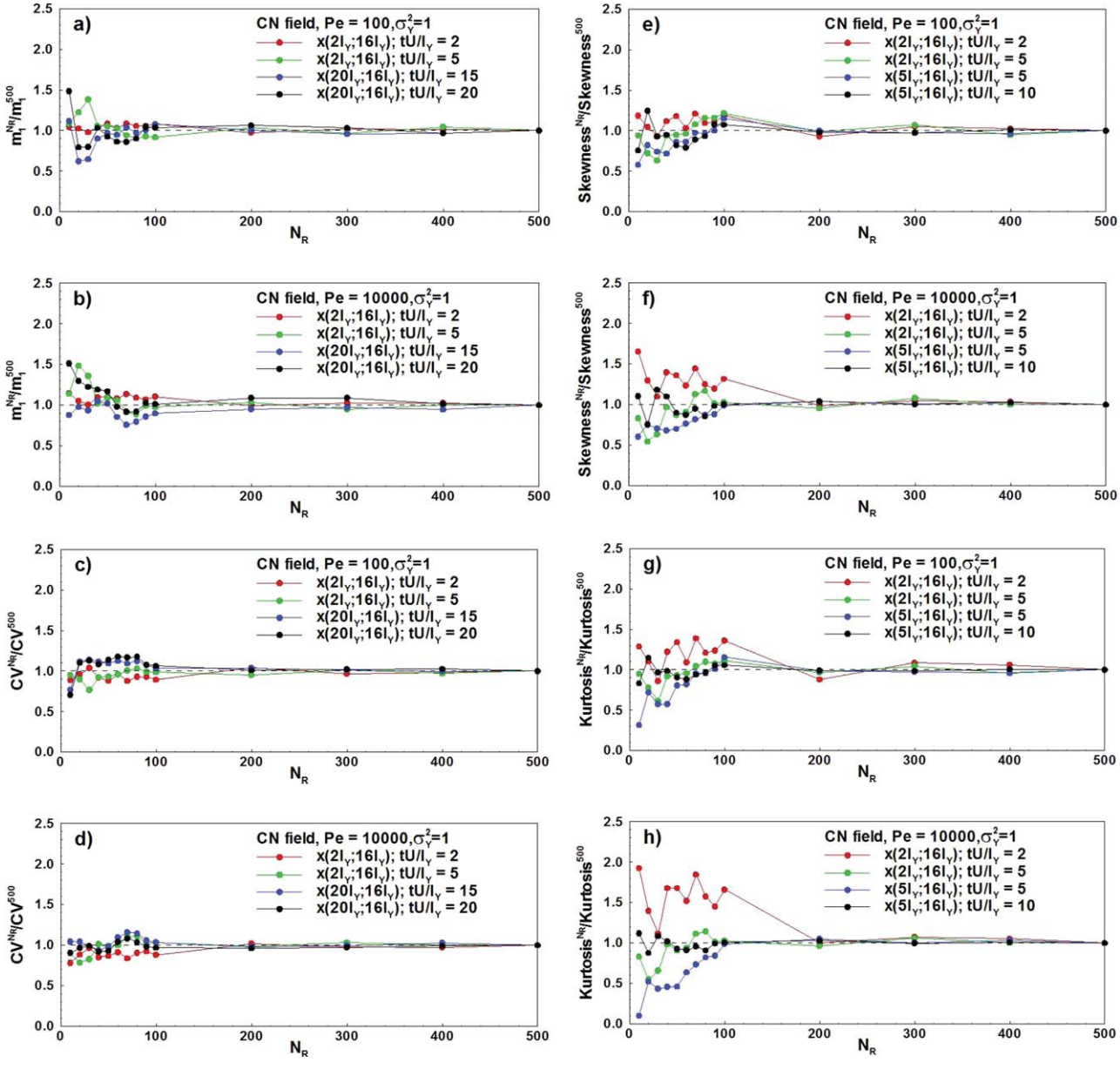

Figure A2. MC convergence study results in case of $\sigma_Y^2 = 1$, CN field; (a) concentration mean, $Pe = 100$, (b) concentration mean, $Pe = 10{,}000$, (c) CV_C, $Pe = 100$, (d) CV_C, $Pe = 10{,}000$, (e) concentration skewness, $Pe = 100$, (f) concentration skewness, $Pe = 10{,}000$, (g) concentration kurtosis, $Pe = 100$, and (h) concentration kurtosis, $Pe = 10{,}000$.

to CV_C, concentration skewness (Figures A1e and A1f) is shown to be higher for a number realizations less than 1000, but for 2000 MC realizations, an approximately constant value is reached. As expected, concentration kurtosis (Figures A1g and A1h) is shown to be most demanding, especially at early and late times. Regardless, the results show stability between 2200 and 2500 MC realizations. At the plume core, differences are less than 0.5%; for early and late arrivals these differences increase but are still less than 3%.

[71] In the case of $\sigma_Y^2 = 1$, 500 MC realizations are shown to be sufficient even for the highest order moments, skewness, and kurtosis. The results are presented in Figures A2a–A2g.

Appendix B: Heterogeneity Grid-Scale Influence

[72] In this section, we compare the first two concentration moments as the mean and CV_C, for two different sets of simulations, conducted for both $I_Y/8$ and $I_Y/4$ heterogeneity scales. Our intention was to follow previously published results; for example, *Ababou et al.* [1989] gave grid criteria $\Delta x/\lambda \leq (1+\sigma_Y^2)^{-1}$ (x presents the mesh size or the heterogeneity grid, while λ denotes the heterogeneity correlation scale) for simulating transport in 3-D heterogeneous porous media. Along these lines, *de Dreuzy et al.* [2007] use 10 grid cells per correlation length for σ_Y^2 up to 9, while *Salandin and Fiorotto* [1998] use 8 grid cells per correlation length. In the work by *Meyer and Tchelepi* [2010], 16 grid

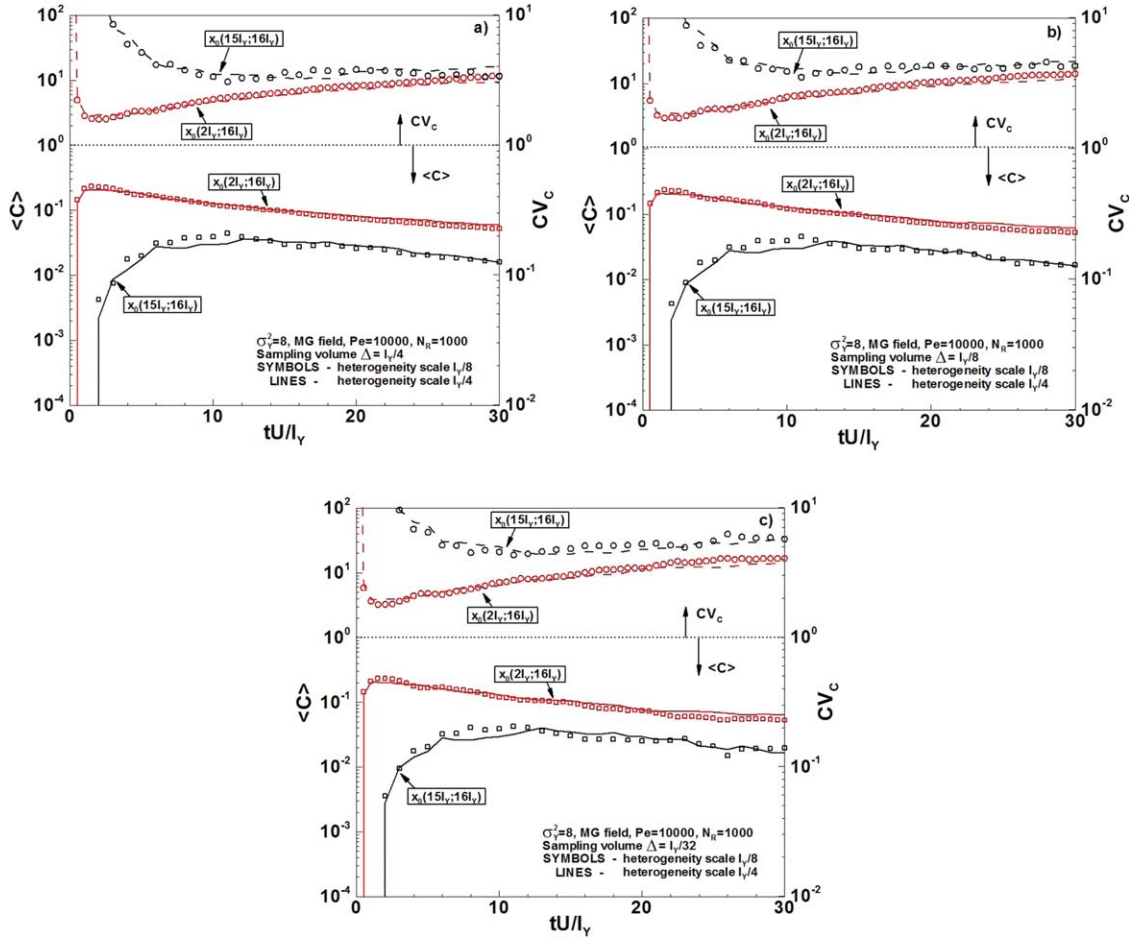

Figure B1. Heterogeneity grid convergence study for $\sigma_Y^2 = 8$, MG field, $Pe = 10{,}000$, $N_R = 1000$, for two sampling locations $2I_Y$ and $15I_Y$ away from source centre along centerline; (a) heterogeneity scale $I_Y/8$ and $I_Y/4$ with sampling size $\Delta = I_Y/4$, (b) heterogeneity scale $I_Y/8$ and $I_Y/4$ with sampling size $\Delta = I_Y/8$, and (c) heterogeneity scale $I_Y/8$ and $I_Y/4$ with sampling size $\Delta = I_Y/32$.

cells per correlation length are used to characterize the heterogeneity field and solve the flow problem for σ_Y^2 up to 4.

[73] We conducted a grid convergence study for the MG field and $\sigma_Y^2 = 8$, with $Pe = 10{,}000$. For these parameters 1000 flow and transport realizations were generated using two discretization levels, $I_Y/8$ and $I_Y/4$.

[74] In Figure B1a we present concentration mean and CV_C for two different sampling locations along the centerline and compare two different heterogeneity scales, $I_Y/8$ and $I_Y/4$, for the sampling volume $I_Y/4$. One can see almost identical moment values near the plume center. Fluctuations are visible for a sampling location $15I_Y$ away from the source, presumably caused by an insufficient number of realizations. In Figure B1b, we did the same but using a smaller sampling volume equal to $I_Y/8$. Moment values for the smallest sampling volume $I_Y/32$ are shown in Figure B1c. As expected, results for CV_C are predominantly influenced by sampling volume. Some differences in CV_C between the two heterogeneity grids are observed as one approaches the plume boundaries. As the sampling volume increases, this difference increases (Figures B1b and B1c). Finally, the earlier observations are consistent with the results presented by *Gotovac et al*. [2009a, Figure 12] where the longitudinal and transversal Eulerian velocity variance is shown as a function of log-conductivity resolution. For the MG field and $\sigma_Y^2 = 2$, discrepancies between $n = 4$ and 8 (number of grid cells per correlation length) are negligible. For $\sigma_Y^2 = 8$ the difference is around 4.5% for both longitudinal and transversal velocity components.

Appendix C: Influence of Sampling Volume on First Two Concentration Moments for DN and CN Log-Conductivity Structures

[75] For this purpose, we use our numerical simulations and extend the sets with two additional sampling volumes $I_Y/2$ and $I_Y/8$. To avoid the mixing caused by local-scale dispersion at the same time, only the case with $Pe = 10{,}000$ is considered. It is shown in Figures C1a–C1d that the impact of the sampling volume on concentration mean at the plume center can be neglected for both DN and CN fields, for $\sigma_Y^2 = 1$ and 8. Moving toward plume fringes some differences are visible in the higher σ_Y^2 case. In contrast to the mean, CV_C is significantly affected by the sampling volume as already

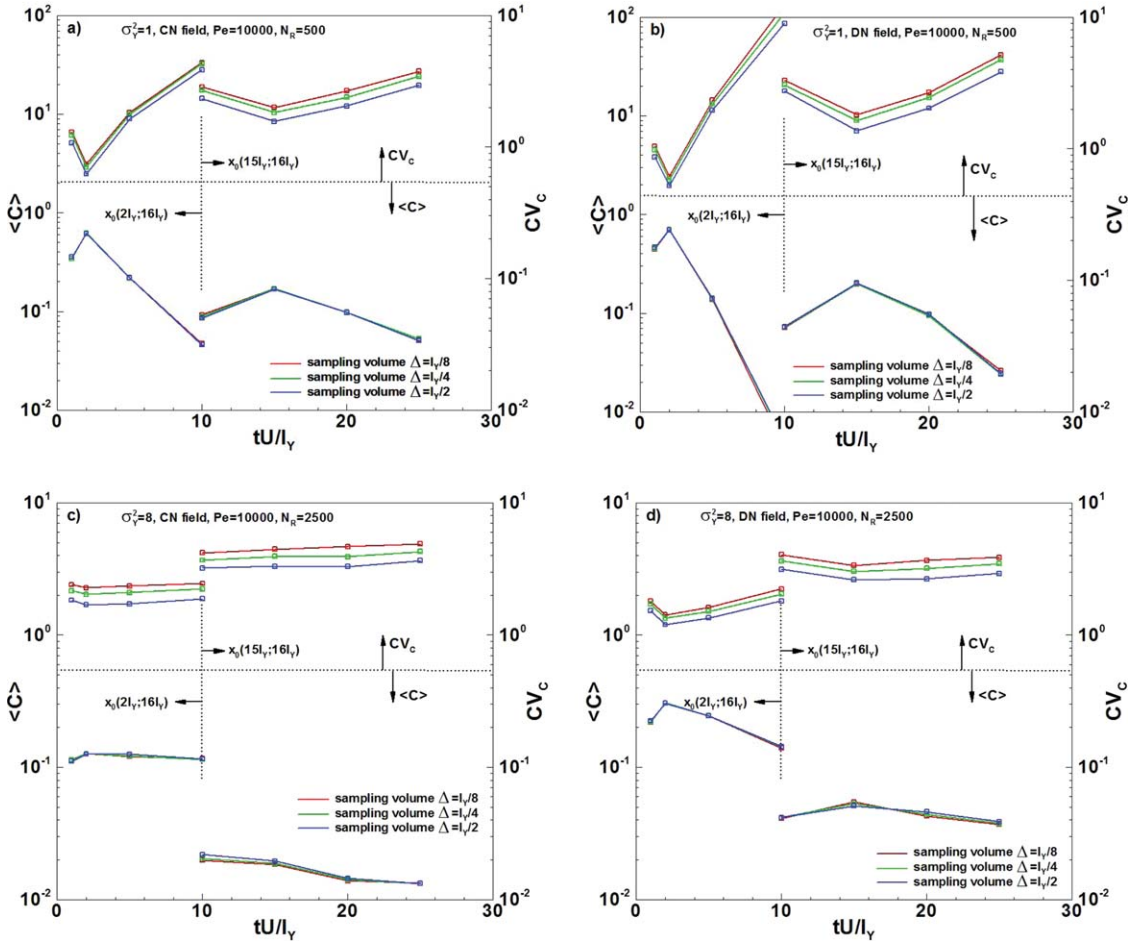

Figure C1. Sampling volume influence ($\Delta = I_Y/8$, $I_Y/4$ and $I_Y/2$) to concentration mean and CV_C, $Pe = 10{,}000$, $N_R = 500$ (2500), for two sampling locations $2I_Y$ and $15I_Y$ away from source centre along centerline, heterogeneity scale $I_Y/4$; (a) $\sigma_Y^2 = 1$, CN field, (b) $\sigma_Y^2 = 1$, DN field, (c) $\sigma_Y^2 = 8$, CN field, and (d) $\sigma_Y^2 = 8$, DN field.

shown for the MG field and small σ_Y^2 [*Andricevic*, 1998; *Tonina and Bellin*, 2008]. As one moves away from the plume center, the impact of the sampling volume further influences the concentration CV_C. CV_C obtained in the CN field is shown to be more sensitive to the sampling volume at the plume core than in the case of the DN field.

References

Ababou, R., D. Mclaughlin, L. W. Gelhar, and A. F. B. Tompson (1989), Numerical simulation of three-dimensional saturated flow in randomly heterogeneous porous media, *Transp. Porous Media*, *4*(6), 549–565.

Andricevic, R. (1998), Effects of local dispersion and sampling volume on the evolution of concentration fluctuations in aquifers, *Water Resour. Res.*, *34*(5),1115–1129.

Andricevic, R. (2008), Exposure concentration statistics in the subsurface transport, *Adv. Water Resour.*, *31*, 714–725.

Andricevic, R., V. Srzic, and H. Gotovac (2012), Risk characterization for toxic chemicals transported in aquifers, *Adv. Water Resour.*, *36*, 86–97, doi:10.1016/j.advwatres.2011.04.009.

Bellin, A., and Y. Rubin (1996), HYDRO_GEN: A spatially distributed random field generator for correlated properties, *Stochastic Hydrol. Hydra*, *10*(4), 253–278.

Bellin, A., and D. Tonina (2007), Probability density function of non-reactive solute concentration in heterogeneous porous formations, *J. Contam. Hydrol.*, *91*, 109–125.

Bellin, A., Y. Rubin, and A. Rinaldo (1994), Eulerian-Lagrangian approach for modeling of flow and transport in heterogeneous geological formations, *Water Resour. Res.*, *30*(11), 2913–2924.

Caroni, E., and V. Fiorotto (2005), Analysis of concentration as sampled in natural aquifers, *Transp. Porous Media*, *59*, 19–45.

Cirpka, O. A., F. P. J. de Barros, G. Chiogna, M. Rolle, and W. Nowak (2011a), Stochastic flux-related analysis of transverse mixing in two dimensional heterogeneous porous media, *Water Resour. Res.*, *47*, W06515, doi:10.1029/2011WR010279.

Cirpka, O. A., F. P. J. de Barros, G. Chiogna, and W. Nowak (2011b), Probability density function of steady state concentration in two-dimensional heterogeneous porous media, *Water Resour. Res.*, *47*, W11523, doi:10.1029/2011WR010750.

Dagan, G. (1982), Stochastic modeling of groundwater flow by unconditional and conditional probabilities: 2. The solute transport, *Water Resour. Res.*, *18*(4), 835–848.

Dagan, G., and A. Fiori (1997), The influence of pore-scale dispersion on concentration statistical moments in transport through heterogeneous aquifers, *Water Resour. Res.*, *33*(7), 1595–1605.

de Dreuzy, J.-R., A. Beaudoin, and J. Erhel (2007), Asymptotic dispersion in 2D heterogeneous porous media determined by parallel numerical simulations, *Water Resour. Res.*, *43*, W10439, doi:10.1029/2006WR005394.

Dentz, M., and D. M. Tartakovsky (2010), Probability density functions for passive scalars dispersed in random velocity fields, *Geophys. Res. Lett.*, *37*, L24406, doi:10.1029/2010GL045748.

Fiori, A. (2003), An asymptotic analysis for determining concentration uncertainty in aquifer transport, *J. Hydrol.*, *284*, 1–12.

Fiori, A., and G. Dagan (2000), Concentration fluctuations in aquifer transport: A rigorous first order solution and applications, *J. Contam. Hydrol.*, *45*, 139–163.

Fiorotto, V., and E. Caroni (2002), Solute concentration statistics in heterogeneous aquifers for finite Peclet numbers, *Transp. Porous Media*, *48*, 331–351.

Fitts, C. R. (1996), Uncertainty in deterministic groundwater transport models due to the assumption of macrodispersive mixing: Evidence from the Cape Cod (Massachusetts, USA) and Borden (Ontario, Canada) tracer tests, *J. Contam. Hydrol.*, *23*, 69–84.

Gotovac, H., R. Andricevic, and B. Gotovac (2007), Multi resolution adaptive modeling of groundwater flow and transport, *Adv. Water Resour.*, *30*(5), 1105–1126.

Gotovac, H., V. Cvetkovic, and R. Andricevic (2009a), Adaptive Fup multi resolution approach to flow and advective transport in highly heterogeneous porous media: Methodology, accuracy and convergence, *Adv. Water Resour.*, *32*, 885–905.

Gotovac, H., V. Cvetkovic, and R. Andricevic (2009b), Flow and travel time statistics in highly heterogeneous porous media, *Water Resour. Res.*, *45*, W07402, doi:10.1029/2008WR007168.

Hassan, E. A., R. Andricevic, and V. Cvetkovic (2001), Computational issues in the determination of solute discharge and implications for comparison to analytical solution, *Adv. Water Resour.*, *24*, 607–619.

Ito, K. (1990), On stochastic differential equations, *Am. Math. Soc.*, *4*, 289–302.

Janković, I., A. Fiori, and G. Dagan (2003), Flow and transport in highly heterogeneous formations: 3. Numerical simulation and comparison with theoretical results, *Water Resour. Res.*, *9*(9), 1270, doi:10.1029/2002WR001721.

Janković, I., A. Fiori, and G. Dagan (2006), Modeling flow and transport in highly heterogeneous three-dimensional aquifers: Ergodicity, Gaussianity and anomalous behaviour: 1. Conceptual issues and numerical simulations, *Water Resour. Res.*, *42*, W06D12, doi:10.1029/2005WR004734.

Kapoor, V., and P. K. Kitanidis (1998), Concentration fluctuations and dilution in aquifers. *Water Resour. Res.*, *34*(5), 1181–1193.

Kinzelbach, W., and G. Uffink (1986), The random walk method and extensions in groundwater modelling, in *Transport Processes in Porous Media*, edited by J. Bear and M. Y. Corapcioglu, pp. 761–787. Kluwer Academic Publishers, London.

Knudby, C., and J. Carrera (2005), On the relationship between indicators of geostatistical, flow and transport connectivity, *Adv. Water Resour.*, *28*, 405–421.

LaBolle, E. M., G. E. Fogg, and A. F. B. Tompson (1996), Random-walk simulation of transport in heterogeneous porous media: Local mass conservation problem and implementation methods, *Water Resour. Res.*, *32*(3), 583–593.

Meyer, D. W., and H. A. Tchelepi (2010), Particle-based transport model with Markovian velocity processes for tracer dispersion in highly heterogeneous porous media, *Water Resour. Res.*, *46*, W11552, doi:10.1029/2009WR008925.

Meyer, D. W., P. Jenny, and H. A. Tchelepi (2010), A joint velocity-concentration PDF method for tracer flow in heterogeneous porous media, *Water Resour. Res.*, *46*, W12522, doi:10.1029/2010WR009450.

Parker, J. C., and M. Th. van Genuchten (1984), Flux-averaged and volume-averaged concentrations in continuum approaches to solute transport, *Water Resour. Res.*, *20*(7), 866–872.

Rubin, Y. (2003), *Applied Stochastic Hydrogeology*, 1st ed., 662 pp., Oxford Press, New York.

Salamon, P., D. Fernandez-Garcia, and J. J. Gomez-Hernandez (2006), A review and numerical assessment of the random walk particle tracking method, *J. Contam. Hydrol.*, *87*, 277–305.

Salandin, P., and V. Fiorotto (1998), Solute transport in highly heterogeneous aquifers, *Water Resour. Res.*, *34*(5), 949–961.

Schwede, R. L., O. A. Cirpka, W. Nowak, and I. Neuweiler (2008), Impact of sampling volume on the probability density function of steady state concentration, *Water Resour. Res.*, *44*, W12433, doi:10.1029/2007WR006668.

Tartakovsky, D. M. (2007), Probabilistic risk analysis in subsurface hydrology, *Geophys. Res. Lett.*, *34*, L05404, doi:10.1029/2007GL029245.

Tonina, D., and A. Bellin (2008), Effects of pore scale dispersion, degree of heterogeneity, sampling size, and source volume on the concentration moments of conservative solutes in heterogeneous formations, *Adv. Water Resour.*, *31*, 339–354.

Wen, X. H., and J. J. Gomez-Hernandez (1998), Numerical modelling of macrodispersion in heterogeneous media: A comparison of multi-Gaussian and non multi-Gaussian models, *J. Contam. Hydrol.*, *30*, 129–156.

Yee (2008), *The concentration probability density function with implications for probabilistic modeling of chemical warfare agent detector responses for source reconstruction, Tech. Rep.,* Defense and Research Development Canada, DRDC Suffield TR 2008-077, 60 pp.

Yee, E. (2009), Probability law of concentration in plumes dispersing in an urban area, *Environ. Fluid Mech.*, *9*, 389–407.

Zheng, C., M. Bianco, and S. M. Gorelick (2010), Lessons learned from 25 years of research at the MADE site, *Ground Water Rev. Pap.*, *49*(5), 649–662, doi:10.1111/j.1745.6584.2010.00753.

Zinn, B., and C. F. Harvey (2003), When good statistical models of aquifer heterogeneity go bad: A comparison of flow, dispersion, and mass transfer in connected and multivariate Gaussian hydraulic conductivity fields, *Water Resour. Res.*, *39*(3), 1051, doi:10.1029/2001WR001146.